Tests of an Ensemble Kalman Filter for Mesoscale and Regional-Scale Data Assimilation. Part III: Comparison with 3DVAR in a Real-Data Case Study

ZHIYONG MENG AND FUQING ZHANG

Department of Atmospheric Sciences, Texas A&M University, College Station, Texas

ABSTRACT

The feasibility of using an ensemble Kalman filter (EnKF) for mesoscale and regional-scale data assimilation has been demonstrated in the authors' recent studies via observing system simulation experiments (OSSEs) both under a perfect-model assumption and in the presence of significant model error. The current study extends the EnKF to assimilate real-data observations for a warm-season mesoscale convective vortex (MCV) event on 10–12 June 2003. Direct comparison between the EnKF and a three-dimensional variational data assimilation (3DVAR) system, both implemented in the Weather Research and Forecasting model (WRF), is carried out. It is found that the EnKF consistently performs better than the 3DVAR method by assimilating either individual or multiple data sources (i.e., sounding, surface, and wind profiler) for this MCV event. Background error covariance plays an important role in the performance of both the EnKF and the 3DVAR system. Proper covariance inflation and the use of different combinations of physical parameterization schemes in different ensemble members (the so-called multischeme ensemble) can significantly improve the EnKF performance. The 3DVAR system can benefit substantially from using short-term ensembles to improve the prior estimate (with the ensemble mean). Noticeable improvement is also achieved by including some flow dependence in the background error covariance of 3DVAR.

1. Introduction

Since the first application of an ensemble Kalman filter (EnKF; Evensen 1994) in the atmospheric sciences field (Houtekamer and Mitchell 1998), the EnKF has been widely examined with different models at different scales and to different realistic extents (Houtekamer and Mitchell 1998; Hamill and Snyder 2000; Anderson 2001; Whitaker and Hamill 2002; Mitchell et al. 2002; Snyder and Zhang 2003; Zhang and Anderson 2003; Zhang et al. 2004, 2006; Aksoy et al. 2005, 2006a,b; Houtekamer et al. 2005; Tong and Xue 2005; Dirren et al. 2007; Meng and Zhang 2007; Whitaker et al. 2008). See Evensen (2003), Lorenc (2003), and Hamill (2006) for a recent review. Studies with simulated observations demonstrate its success at decreasing forecast error and its better performance relative to variational data assimilation methods such as three-dimensional variational data assimilation (3DVAR) in

a large-scale model (Hamill and Whitaker 2005) and four-dimensional variational data assimilation (4DVAR) in later cycles in a cloud model especially for model variables not functionally related to the observations (Caya et al. 2005).

One of the difficulties in real-world applications of ensemble-based data assimilation techniques is the proper representation of model error (Zhang and Snyder 2007). Recently, progress has been made in accounting for model error by using additive or multiplicative covariance inflation (Hamill and Whitaker 2005; Houtekamer et al. 2005; Barker 2005). For example, encouraging results in real-data applications have been obtained in an ocean general circulation model (Keppenne and Rienecker 2002), as well as global (Whitaker et al. 2004, 2008; Houtekamer et al. 2005) and limited-area models (Dowell et al. 2004; Barker 2005; Fujita et al. 2005). The performance of the EnKF implemented in global models with real data has been shown to be better than (Whitaker et al. 2004, 2008) or at least comparable to that of the 3DVAR method (Houtekamer et al. 2005). However, direct comparison between an EnKF and 3DVAR in limited-area models has not been seen in the literature, which will be a focus of this study.

Corresponding author address: Dr. Fuqing Zhang, Dept. of Atmospheric Sciences, Texas A&M University, College Station, TX 77845-3150.
E-mail: fzhang@tamu.edu

In Zhang et al. (2006, Part I of this series), the performance of an EnKF implemented in the fifth-generation Pennsylvania State University–National Center for Atmospheric Research Mesoscale Model (MM5) was examined with the perfect-model assumption by assimilating synthetic sounding and surface observations with typical temporal and spatial resolutions (Part I). It was found that the EnKF with 40 members works very effectively in keeping the analysis close to the truth simulation. Most error reduction comes from the large scale, which is consistent with Daley and Menard (1993), though different mechanisms are involved in their study. Furthermore, the EnKF performs differently for different variables; it is least effective for vertical motion and moisture because of their relatively strong smaller-scale components, but it is the most effective in reducing the error in pressure (and also very effective, but to a lesser degree, for horizontal winds and temperature) because of its dominant larger-scale components (Part I).

Subsequently in Meng and Zhang (2007, Part II in this series), the performance of the EnKF was investigated in the presence of model error because of imperfect subgrid physical parameterization schemes. The result shows that the EnKF still performs reasonably well, though its performance can sometimes be significantly degraded by the presence of model error. It was found that using different combinations of different physical parameterization schemes in different ensemble members can significantly improve filter performance as a result of the better background error covariance and mean estimation. Different performance levels of this EnKF system were also observed for different flow regimes (Part II).

As a natural extension of these two observation simulation system experiment (OSSE) studies under both perfect and imperfect model assumptions, the current study implements the same EnKF in the Weather Research and Forecasting Model (WRF) for real-world data assimilation for the same mesoscale convective vortex (MCV) event. Its performance is directly compared with the three-dimensional variational data assimilation system of the WRF (WRF-3DVAR), complementary to similar comparisons performed with global models (Houtekamer et al. 2005; Whitaker et al. 2008). In the next section, a brief introduction is given concerning the methodology, including the model, the EnKF, and the 3DVAR method. The synoptic overview of the MCV event and the observations to be assimilated are described in section 3. Section 4 compares the performance of the EnKF and the 3DVAR method. Sensitivities of both methods to the background error covariance are examined in section 5. A brief summary and discussion are given in section 6.

2. Methodology

a. The mesoscale model

The Advanced Research WRF (ARW) is used in this study. WRF is a fully compressible, nonhydrostatic mesoscale model (Skamarock et al. 2005). The vertical coordinate follows the terrain using hydrostatic pressure, and the model uses an Arakawa C grid. Prognostic variables are column mass of dry air (μ_d), velocity (u, v, and w), potential temperature (θ), geopotential (ϕ), and mixing ratios for water vapor (q_v), cloud (q_c), rain (q_r), ice (q_i), snow (q_s), and grauple (q_g).

In this work, two domains with one-way nesting are used. The coarse domain covers the contiguous United States with 64×45 grid points and a grid spacing of 90 km, and the inner domain covers the central United States with 76×61 grid points and a grid spacing of 30 km (Fig. 1a). Both model domains have 27 vertical layers, and the model top is set at 100 hPa. Unless otherwise specified, the physical parameterization schemes include the Grell–Devenyi cumulus scheme (Grell and Devenyi 2002), the WRF Single Moment (WSM) six-class microphysics with graupel (Hong et al. 2004), and the Yonsei State University (YSU) scheme (Noh et al. 2003) for planetary boundary layer (PBL) processes. National Centers for Environmental Prediction (NCEP) global final (FNL) analyses are used to create initial and boundary conditions. Data assimilation and verification are only performed in the inner domain.

b. WRF-3DVAR

The WRF-3DVAR method used here was developed primarily at NCAR, and it is now operational at the Air Force Weather Agency (Barker et al. 2004). Its configuration is based on an incremental formulation, producing a multivariate analysis in the model space. Its incremental cost function is minimized in a preconditioned control variable space where the errors of different control variables are largely uncorrelated.

WRF-3DVAR has several background error statistic (BES) options for control variables ("cv"). The "cv3" option formulates physical-space control variables, namely streamfunction, unbalanced velocity potential, unbalanced surface pressure, unbalanced temperature, and "pseudo" relative humidity. The "cv5" option formulates eigenvector-space control variables, namely streamfuction, velocity potential, unbalanced pressure, and relative humidity (Xiao and Sun 2007).
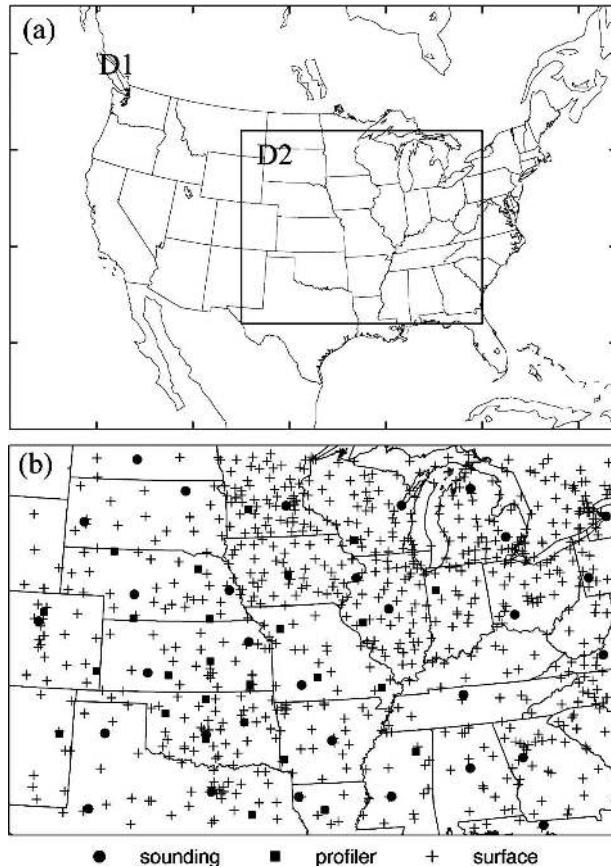
FIG. 1. (a) Map of the model domain and (b) distribution of the assimilated observations in domain 2.

After minimization in control space, the control vector is then projected to the model grid via a recursive filter in the horizontal direction and EOF transformation in the vertical direction. Then, physical variable transformation is performed using a balance equation. In detail, wind increments are calculated from the streamfunction and velocity potential. Balanced mass increments are obtained through linearized geostrophic and cyclostrophic mass–wind balance equations (Barker et al. 2004).

As in any other data assimilation technique, the structure of the background error covariance plays a very important role in 3DVAR. The WRF-3DVAR background error covariance may be estimated via the so-called National Meteorological Center model [NMC, now operating as NCEP; Parrish and Derber (1992)], which uses the statistics of the differences between at least 1 month of 24- and 12-h forecasts valid at the same time. Alternatively, deviations of individual members from the mean of a short-term ensemble can be used, which may improve the representation of smaller-scale features (Lee and Barker 2005). Sensitiv-

ity of the performance of 3DVAR to different representations of background error statistics will be examined in section 5.

c. The EnKF

The EnKF is the same as that in Parts I and II except for being implemented in the WRF model, which uses the covariance relaxation of Zhang et al. (2004) to inflate the background error covariance. Unlike the standard inflation method (Anderson 2001), in which all points in the prior field are inflated, this relaxation method only inflates the covariance at updated points via a weighted average between the prior perturbation (denoted by superscript f) and the posterior perturbation (denoted by superscript a) as follows:

$$(\mathbf{x}_{\text{new}}^a)' = (1 - \alpha)(\mathbf{x}^a)' + \alpha(\mathbf{x}^f)'. \tag{1}$$

The weighting coefficient α is set to 0.5 in the OSSE studies in Parts I and II. Considering that prior error in real-data application may be larger because of the unavoidable imperfectness of the forecast model, a value of 0.7 is used here unless otherwise specified. The Gaspari and Cohn (1999) fifth-order correlation function with a radius of influence of 30 (10) grid points [i.e., 900 km (300 km)] for soundings and profilers (surface observations) in horizontal directions and 15 sigma levels in vertical directions is used for covariance localization. Although the optimum ensemble size to estimate the forecast uncertainty is still under active research, 40 members are used herein. This is both affordable and reasonable based on previous studies (e.g., Houtekamer and Mitchell 2001; Anderson 2001; Snyder and Zhang 2003; Zhang 2005; Part I; Part II).

d. Ensemble initial and boundary perturbations

As in Part I, the initial ensemble is generated with the WRF-3DVAR (Barker et al. 2004) using the BES of option cv3. To create a largely balanced perturbation, we first generate a set of random control vectors with a normal distribution (zero mean and unit standard deviation). Then, the control increment vector is transformed back to model space via an EOF transform, a recursive filter, and physical transformation via balance equation. The perturbed variables include the horizontal wind components, potential temperature, and mixing ratio for water vapor whose error statistics are defined by the climatological background error covariance. Other prognostic variables such as vertical velocity (w) and mixing ratios for cloud water (q_c), rainwater (q_r), snow (q_s), and graupel (q_g) are not perturbed. The perturbation standard deviations thus gen-

erated are approximately 2 m s^{-1} for the horizontal wind components (u and v), 1 K for the potential temperature (T), 1 hPa for the pressure perturbation (p'), and 0.5 g kg^{-1} for the water vapor mixing ratio (q). The 3DVAR perturbations are added to the GFS FNL analysis to form an initial ensemble, which is then integrated for 12 h to develop an approximately realistic, flow-dependent background error covariance structure before the first observation is assimilated. Similar methods, using 3DVAR to generate the initial ensemble for the EnKF, are also employed in Houtekamer et al. (2005) and Barker (2005).

The simplest way to perturb lateral boundary conditions for a limited-area model is to use a global ensemble forecast with the correct size and resolution (which is usually unavailable; Chessa et al. 2004). Torn et al. (2006) examined several alternative boundary perturbation methods and concluded that the error originating from using different methods is limited to near the edges of the domain. In this paper, the GFS FNL analyses at different times used to create boundary conditions are perturbed in the same manner as with the initial ensemble.

3. Overview of the MCV event and observations to be assimilated

a. The MCV event in BAMEX

The case of interest is an MCV event that occurred during an intense observation period (IOP8) of the Bow Echo and Mesoscale Convective Vortex Experiment (BAMEX) conducted from 18 May to 7 July 2003 over the central United States (Davis et al. 2004). This event exhibited typical environmental features common to long-lived MCVs such as weak shear and moderate environmental instability (Trier et al. 2006; Hawblitzel et al. 2007; Davis and Trier 2007; Trier and Davis 2007). At 0000 UTC 10 June 2003, a disturbance embedded in the subtropical jet triggered convections over eastern New Mexico and western Texas. An MCV developed from the remnants of this convection over central Okalahoma at 0600 UTC 11 June 2003 and matured by 1800 UTC 11 June (with a bow echo occurring at western Tennessee) as it traveled northeastward toward Missouri and Arkansas (Hawblitzel et al. 2007, their Fig. 2). Its circulation was about 400 km wide and possessed a well-defined PV maximum around 600 hPa with a cold anomaly below the circulation and a warm anomaly above it. This MCV seemed to help initiate widespread convection on its downshear side at 1600 UTC and on the north side of the circulation at 2200 UTC. Most convection died by 0000 UTC 12 June, and the MCV then transitioned into an extratropical baroclinic system (Hawblitzel et al. 2007).

b. Observations to be assimilated

The observations to be assimilated in this study include sounding, surface, and wind profiler observations located in domain 2 (Fig. 1b). Wind profilers (denoted by filled squares) are distributed mainly in central United States to fill the gaps between radiosondes. They have previously proven to be effective in improving short-range (3–12 h) forecasts (Benjamin et al. 2004). Data thinning is performed here on the profiler observations so that the vertical resolution is similar to that of typical soundings.

Here, we use a quality control method similar to a procedure in Barker (2005) that guarantees that 3DVAR and the EnKF assimilate exactly the same observations. First, the FNL analysis fields are interpolated to the model grid at 6-h intervals. Then, the model is integrated for 6 h starting from the 6-hourly initial condition. An hourly database is then formed by combining the interpolated 6-hourly FNL analyses at 0000, 0600, 1200, and 1800 UTC with hourly WRF forecasts in between including 0100–0500, 0700–1100, and 1300–1700 UTC for each day of interest. This hourly database is then used as the first guess for a prerun of WRF-3DVAR to assimilate observations generated by the observation preprocessor of WRF-3DVAR. The data processed at hourly intervals that have been ingested by this prerun will then be assimilated by the following 3DVAR and EnKF experiments. The output file containing the ingested observations transforms the original wind speed, wind direction, and relative humidity into horizontal wind components (u and v) and the mixing ratio of the water vapor (q). Consequently, the assimilated variables become horizontal wind components (u and v), temperature (T), and the mixing ratio of the water vapor (q) for soundings; surface pressure (ps), u, v, T, and q for surface data; and u and v for wind profiler data. In this way, the observations first go through a basic quality control process such as range, domain, persistency, extreme-value, and buddy checks. Then, in the 3DVAR prerun, an "errormax" quality control is performed by dropping the observations whose absolute differences from the first guess are more than five times larger than the corresponding observation errors.

The observation errors of the soundings and wind profilers are given in Table 1. The observation errors of the surface data are 2 K for temperature, 10% for relative humidity, and 100 Pa for surface pressure (Barker et al. 2004).

TABLE 1. Observation error for sounding and profiler.

Pressure (hPa)	100	150	200	250	300	400	500	700	850	1000
Wind (m s^{-1})										
Sounding	2.7	3.0	3.3	3.3	3.3	2.8	2.3	1.4	1.1	1.1
Profiler	2.8	2.8	3.0	3.1	3.2	3.0	2.8	2.2	2.2	2.2
Temperature (K)	1	1	1	1	1	1	1	1	1	1
RH (%)	10	10	10	10	10	10	10	10	10	15

4. Comparison between the EnKF and 3DVAR

a. The reference forecasts

With the initial and boundary conditions interpolated from the FNL analysis, a 36-h reference deterministic forecast (DF) is conducted starting from 1200 UTC 10 June 2003 without assimilating any observations. In comparison with the observation (Fig. 2a), the simulated MCV (Fig. 2b) moves much faster, resulting in a position error of about 400 km at 0000 UTC 12 June.

To assess the benefit of the EnKF from both the data assimilation algorithm itself and the utilization of the ensemble forecast for state estimate, a 36-h reference ensemble forecast is also performed with the same model configuration for all members as that in the DF but with the addition of initial and boundary perturbations described in section 2d (hereinafter also referred to as EF). Relative to the DF, the mean of EF shows slightly smaller error in the 36-h surface location of the simulated MCV (Fig. 2c). The magnitude of its simulated reflectivity is lower because of the ensemble averaging.

The error of the reference EF is smaller than that of DF in terms of column-averaged root-mean difference total energy (RM-DTE) and root-mean-square (RMS) error (RMSE) of q verified against sounding observations (Figs. 3a–d). The DTE is defined as in Zhang (2005):

$$DTE = 0.5(u'u' + v'v' + kT'T'), \qquad (2)$$

where the primes denote the differences between the observations and the verified fields and $k = C_p/T_r$, with $C_p = 1004.7$ J kg^{-1} K^{-1} and the reference temperature $T_r = 290$ K. Figure 3 also shows that the largest errors in both reference forecasts occur around the MCV.
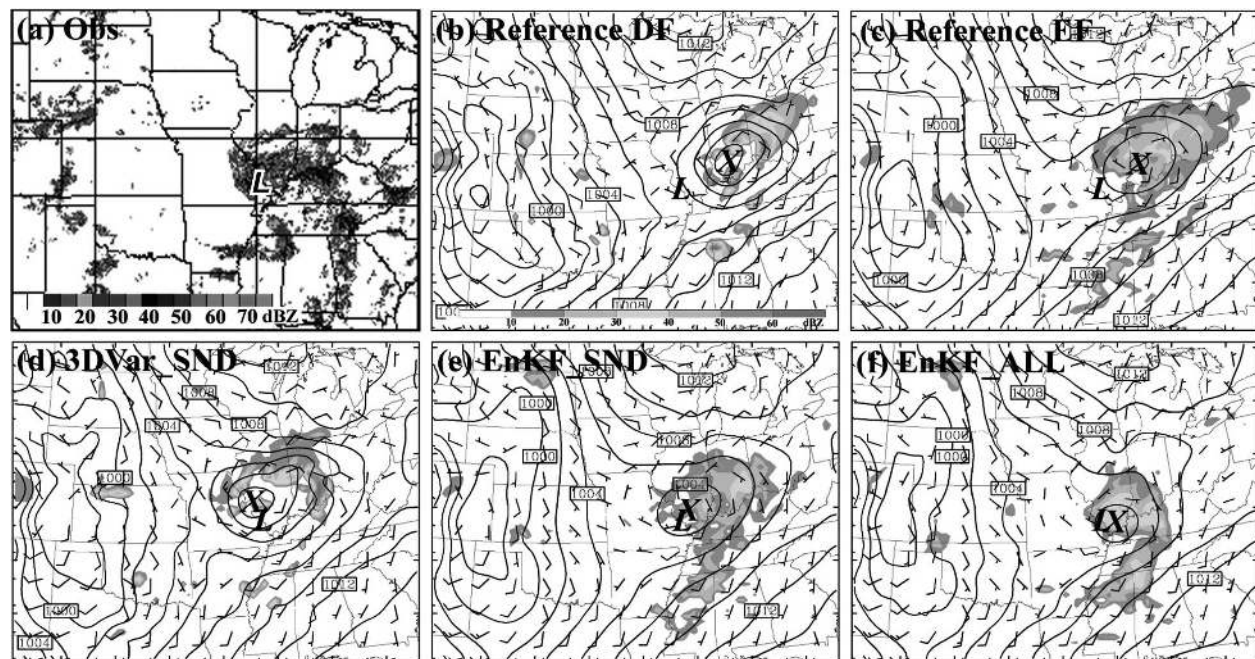

FIG. 2. (a) Observed radar echoes at 0000 UTC 12 Jun. The MSLP (every 2 hPa), 10-m wind vectors (full barb 5 m s^{-1}), and simulated reflectivity (shaded) valid at 36 h (0000 UTC 12 Jun) of the reference forecasts (b) DF and (c) EF and the prior forecast of (d) 3DVAR_SND, (e) EnKF_SND, and (f) EnKF_ALL. The X and L, respectively, denote the simulated and observed MCV centers at the surface.
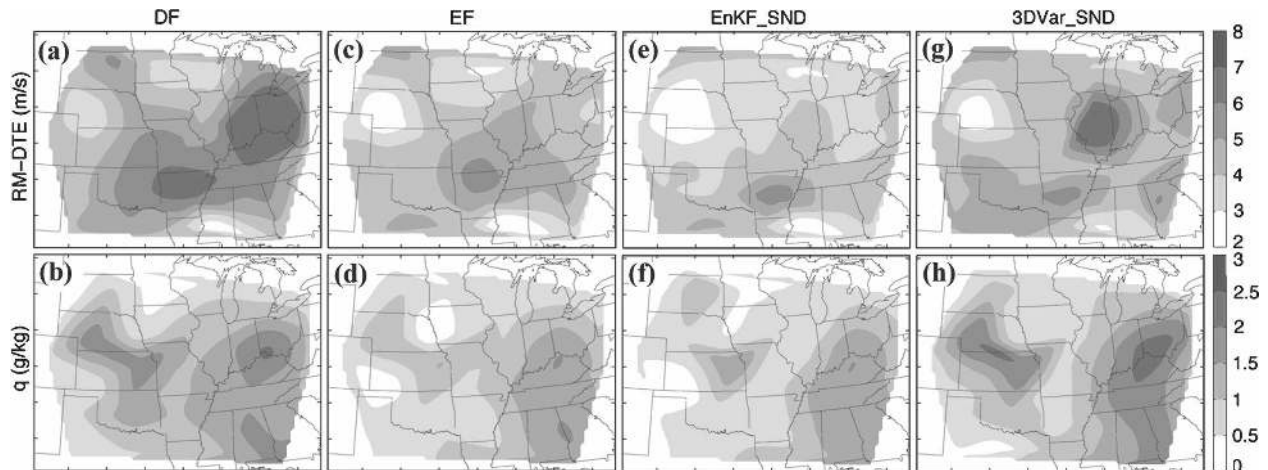
FIG. 3. Horizontal distributions of the column-averaged RM-DTE and RMSE of *q* valid at 36 h for the reference forecast (a),(b) DF and (c),(d) EF and the prior forecast of (e),(f) EnKF_SND and (g),(h) 3DVAR_SND.

b. Experiments with different types of observations

Three types of observations including sounding, surface, and wind profiler data are assimilated separately via both the EnKF and 3DVAR in this section. The experiments are named "EnKF_SND" and "3DVAR_SND" for sounding assimilation, "EnKF_SFC" and "3DVAR_SFC" for surface assimilation, and "EnKF_PFL" and "3DVAR_PFL" for profiler assimilation. As mentioned before, all results are verified against soundings that have passed our quality control procedure at nine standard pressure levels, that is, 925, 850, 700, 500, 400, 300, 250, 200, and 150 hPa, unless otherwise specified.

1) SOUNDING DATA

The results show that the EnKF very efficiently draws the analysis close to the observations (black dot–dashed line in Fig. 4) for the 30 sounding sites within the inner (assimilation and verification) domain where *u*, *v*, *T*, *q*, and ps are assimilated every 12 h. At each data assimilation time, the posterior RMSE (black dot–dashed line in Fig. 4) is smaller than the prior RMSE (black solid line in Fig. 4) by up to 50%. However, since the verification of the analysis (posterior) uses the same sounding observations as those assimilated, it is more appropriate to judge the performance of the data assimilation via the short-term forecast (prior estimate) initialized with the posterior analysis from the previous assimilation cycle. The EnKF prior estimate (black solid line in Fig. 4) at 36 h also tracks the observations better than both the reference DF (gray dashed line in Fig. 4) and EF (black dashed line in Fig. 4). Similar to the results obtained in OSSE studies (Part I; Part II),

larger improvements are observed in variables with higher power at large scales such as *u*, *v*, and *T*. After two cycles at 36 h, the prior RMSEs of *u*, *v*, and *T* are, respectively, 3.3 m s^{-1}, 4.0 m s^{-1}, and 1.8 K. The RMSE of *q* grows faster than do other variables during the subsequent integrations, likely because of its higher spectral power at smaller scales (Part I).

In comparison with EnKF_SND, much worse performance is seen in 3DVAR_SND. Though its prior RMSEs at 36 h (gray solid line in Fig. 4) are smaller than those of the reference DF, they are much larger than those of EnKF_SND and even slightly larger than the RMSEs of the reference EF for all *u*, *v*, *T*, and *q*. The posterior errors (gray dot–dashed line in Fig. 4) of *u* and *v* at 36h are also noticeably larger than those of EnKF_SND. The errors grow much faster in the 3DVAR 12-h forecasts than in the EnKF. This result is consistent with the better performance of a global model–based EnKF relative to 3DVAR by assimilating the operational observation network of NCEP except for satellite data (Whitaker et al. 2008).

The better performance of the EnKF relative to 3DVAR can also be seen in the vertical distribution of domain-averaged prior RMSEs of *u*, *v*, *T*, and *q* at 36 h (Fig. 5). The errors of 3DVAR (gray solid line in Fig. 5) are generally larger than those of the EnKF (black solid line in Fig. 5) in each layer with local maxima near the tropopause and the surface. Most of the error reduction of the EnKF relative to the reference EF comes from the lower troposphere. Examination of the horizontal distribution of the column-averaged prior error shows that the EnKF performs significantly better than does 3DVAR over the MCV area (Figs. 3 e–h).

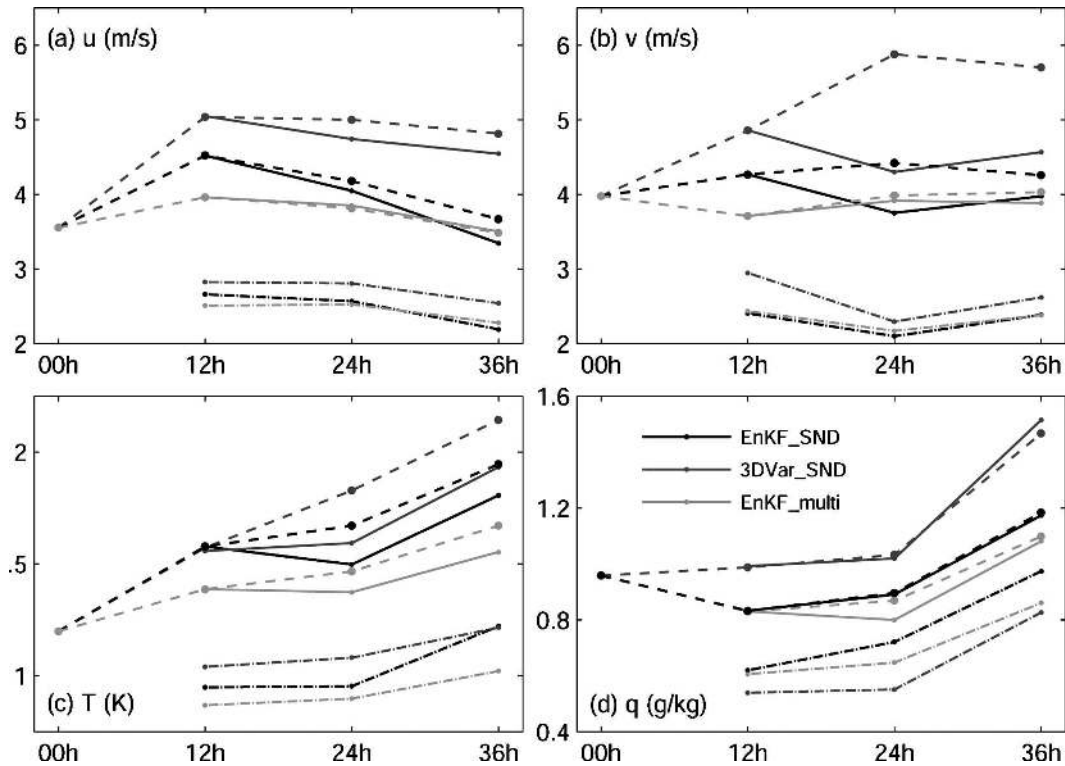EnKF_SND also draws the simulated MCV closer to

FIG. 4. Time evolution of domain-averaged RMSEs of (a) u, (b) v, (c) T, and (d) q for EnKF_SND (black), 3DVAR_SND (gray), and EnKF_multi (light gray). The solid lines denote the prior RMSEs, and the dot–dashed lines are the posterior RMSEs. Also plotted are the RMSEs of the reference forecast DF (gray dashed), EF (black dashed), and EF_multi (light gray dashed).

the observed location (Fig. 2e) than do either the reference forecasts or 3DVAR (Figs. 2b–d). The simulated reflectivity is slightly stronger and better organized (especially to the south of the surface center) than that in the reference EF and much closer to the observed location (Fig. 2a). When compared with the reference DF (Fig. 2b), 3DVAR_SND (Fig. 2d) also better simulates the position of the MCV and its associated reflectivity.

The domain-averaged RM-DTEs of forecasts and analyses of all experiments at 36 h (Fig. 6) clearly show that EnKF_SND performs better than 3DVAR_SND. Also shown is that EnKF_SND performs better than references EF and DF, while 3DVAR_SND performs better than reference DF but worse than reference EF. The RM-DTE of EnKF_SND is 4.38 m s^{-1} while that of 3DVAR_SND is 5.19 m s^{-1}. Results from other experiments also shown in Fig. 6 will be discussed in subsequent sections.

To further investigate the capability of these two methods in depicting the MCV structure, short-term forecasts started from the 3DVAR analysis and ensemble analyses at 1200 UTC 11 June are verified against 20 dropsonde observations obtained during

IOP8 of BAMEX from 1604 to 1905 UTC 11 June at approximately 8-min intervals. These dropsonde observations are taken in and around the area of the MCV and have passed a basic quality control through the preprocessor of WRF-3DVAR. In particular, comparison of the simulated wind vectors from both analyses with the dropsonde observations at 1730 UTC (approximately the averaged dropsonde time) shows that the EnKF forecast captures the MCV circulation better than does 3DVAR with a closed midlevel vortex in the observed location (Fig. 7). The domain-averaged RMSEs of u, v, T, and q verified against the dropsonde observations at the nearest half or integer hour model output times from 1600 to 1900 UTC (Fig. 8) show that EnKF_SND (black lines) apparently has smaller error than does 3DVAR_SND (gray lines) in both dynamic and thermodynamic variables but more so in the wind fields.

Further improvement in T and q can be achieved through including model physics parameterization uncertainties in the ensemble forecast to be discussed in section 5a. Also discussed later is that the better performance of the EnKF when compared with 3DVAR may come from using both the ensemble mean for prior
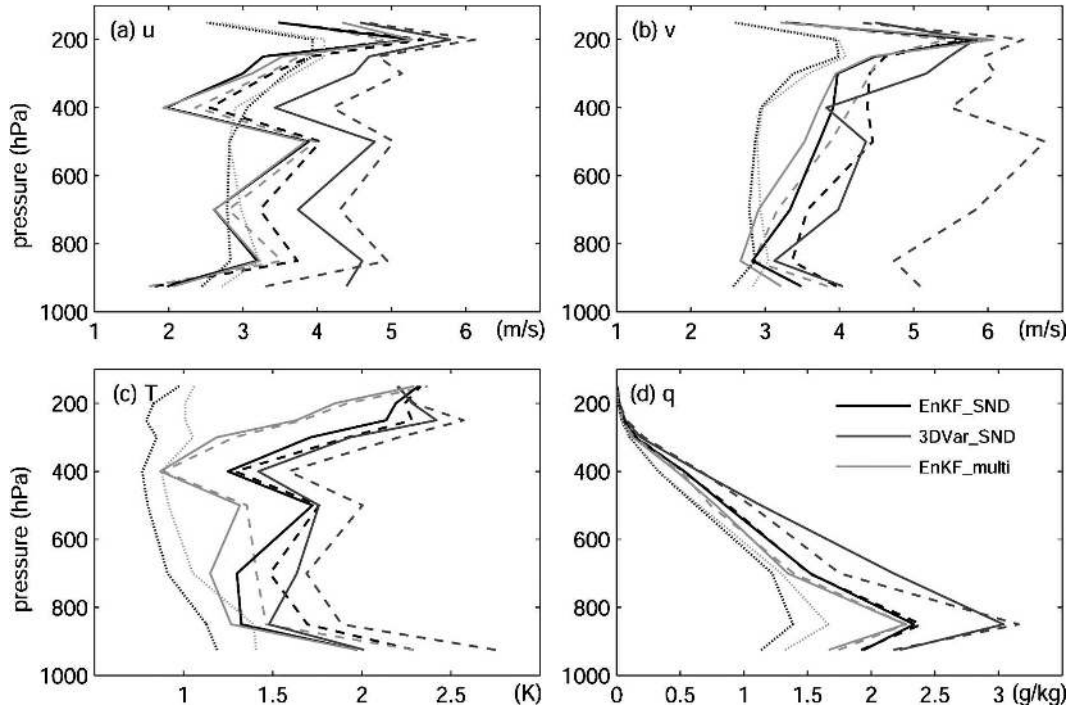
FIG. 5. Vertical distributions of the horizontally averaged prior RMSEs of (a) u, (b) v, (c) T, and (d) q for EnKF_SND (black solid), 3DVAR_SND (gray solid), and EnKF_multi (light gray solid). Also plotted are the horizontally averaged prior ensemble spreads (STD) of EnKF_SND (black dotted) and EnKF_multi (light gray dotted) together with the horizontally averaged RMSEs of the reference forecast DF (gray dashed), EF (black dashed), and EF_multi (light gray dashed).
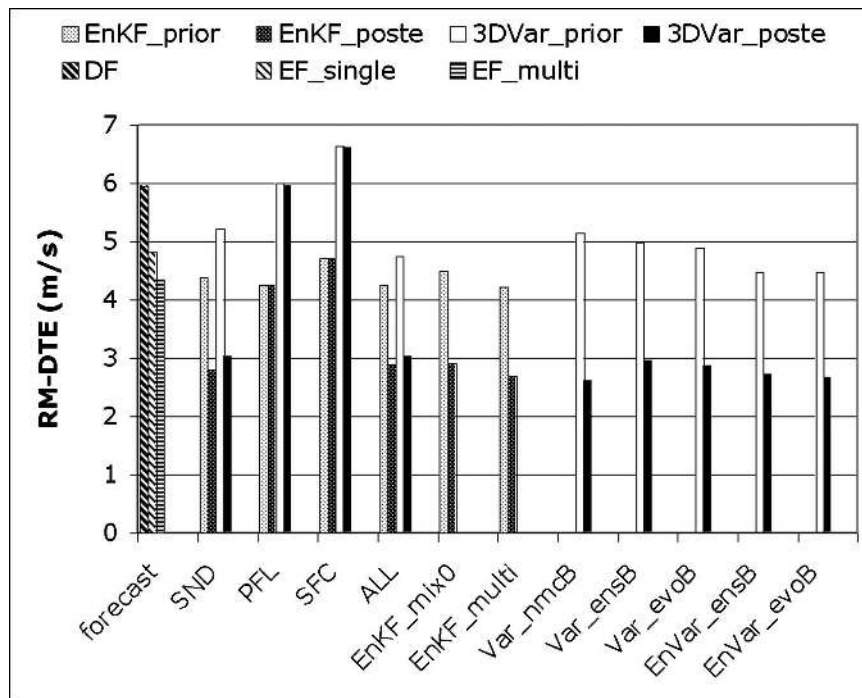

FIG. 6. A summary of domain-averaged RM_DTE prior/forecast and posterior/analysis errors valid at 36 h for all experiments.
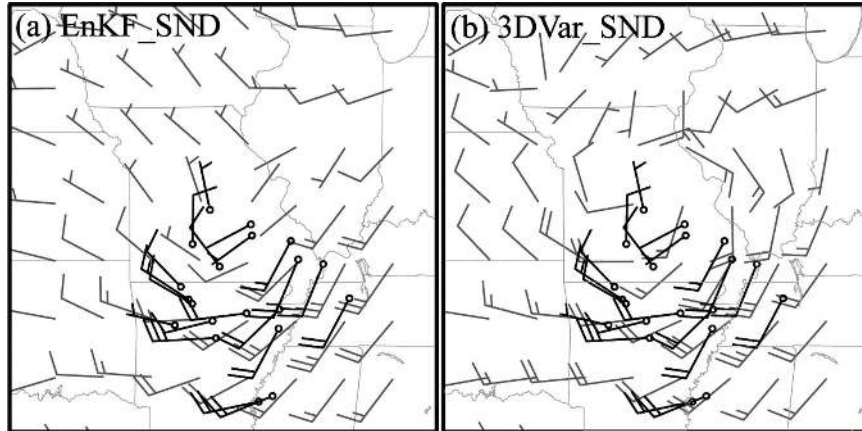
FIG. 7. Wind vector forecast (gray color) at 700 hPa of (a) EnKF_SND and (b) 3DVAR_SND valid at 1730 UTC 11 Jun 2003 starting from their respective posteriors at 1112 UTC 11 Jun. The dropsonde observation during 1604–1905 UTC 11 Jun are plotted in black.

estimation and a flow-dependent background error covariance. Note that the ensemble mean is used for the EnKF to calculate the RMSEs but a single realization is used for 3DVAR. The ensemble mean fields do not likely have the same variability as the 3DVAR single realization and smooth fields will have a systematic advantage in the RMSE-based scores. For example, application of a standard five-point smoother once to the 12-h forecast of the 3DVAR single-run forecast at 36 h may reduce the domain-averaged RM-DTE from 5.2 to 5.1 m s^{-1} and further to 4.8 m s^{-1} after applying 10 smoother times. However, the RM-DTE from the smoothed 3DVAR forecast is still significantly larger than that of EnKF_SND, 4.4 m s^{-1} (4.2 m s^{-1} for
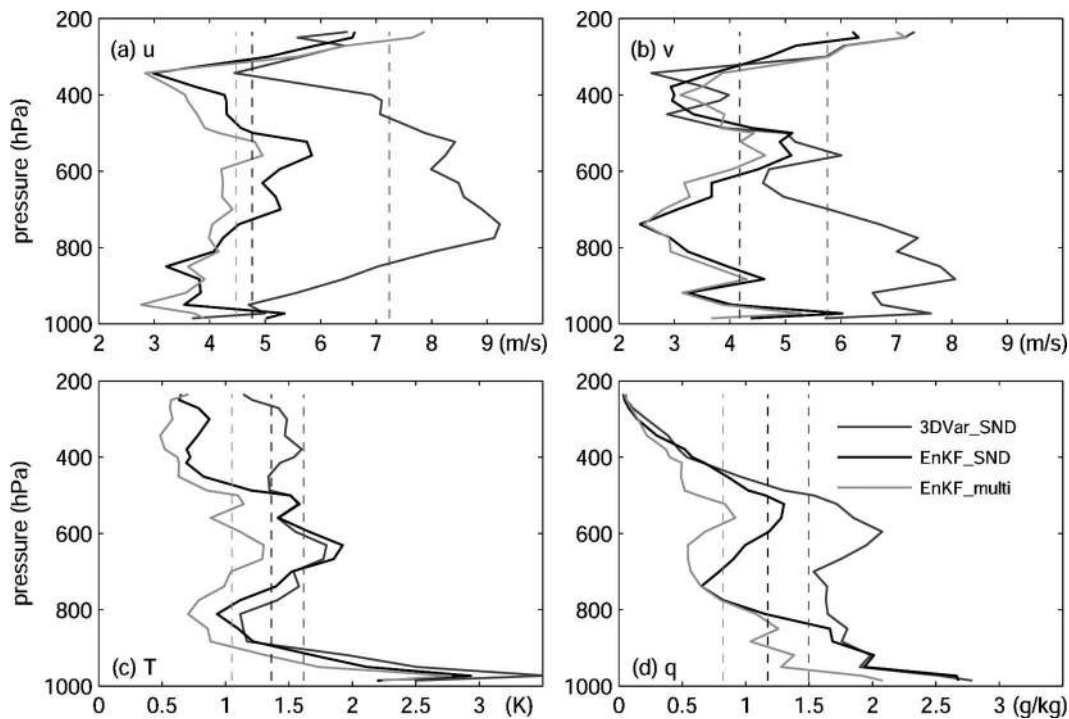

FIG. 8. Vertical distributions of the horizontally averaged RMSEs of (a) u, (b) v, (c) T, and (d) q of forecasts over 1600–1900 UTC starting from their respective posteriors of EnKF_SND (black), EnKF_multi (light gray), and 3DVAR_SND (gray) at 1200 UTC 11 Jun. The straight vertical lines denote the respective domain-averaged RMSEs over the same period.
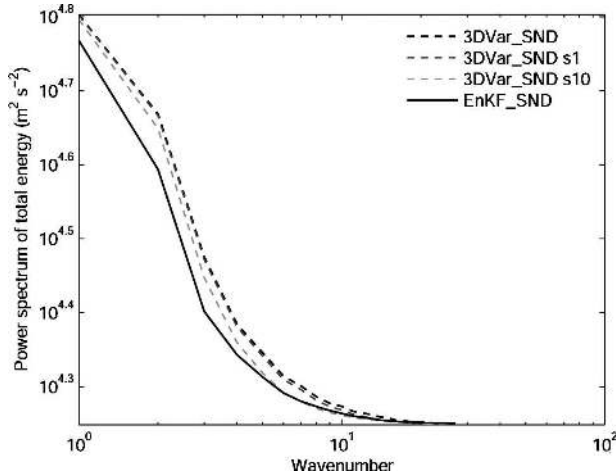
FIG. 9. Power spectral analyses of the prior-forecast total energy at 0000 UTC 12 Jun for 3DVAR_SND with 0, 1, and 10 times of five-point smoothing (black dashed, gray dashed, and light gray dashed, respectively), and EnKF_SND (black solid).

EnKF_muti; section 5a). Power spectrum analyses of the prior-forecast total energy at 0000 UTC 12 June in Fig. 9 show that the total energy of 3DVAR_SND will decrease slightly at smaller scales after one application of a five-point smoother. A much greater reduction of the total energy at smaller scales can be further achieved after applying the five-point smoother 10 times, but the reduction of the variability at larger scales is only marginal compared to that of the ensemble mean forecast of EnKF_SND (Fig. 9). This result suggests that the difference in performance between 3DVAR_SND and EnKF_SND is not solely because of the averaging/smoothing effects implicit in the EnKF approach.

2) WIND PROFILER

While the 28 profilers in the inner domain with u and v observations take observations as frequent as every 6 min (Fig. 1b), profiler data assimilation was only performed every 3 h. Testing showed no benefit (in terms of analysis error) in assimilating profiler data more often than every 3 h. The reason for this frequency limit is not exactly clear but it could be that an even smaller assimilation window might be too short for the ensemble to develop additional meaningful error covariance structures while imbalance from previous analysis cycle may not have sufficient time to be dispersed. Assimilating more frequent observations with similar information content is more vulnerable to sampling errors given the limited ensemble size.

In comparison with EnKF_SND, EnKF_PFL has a slightly smaller prior RM-DTE at 36 h (4.25 m s^{-1} ver-

sus 4.38 m s^{-1} in Fig. 6), likely because the previous assimilation cycle was only 3 h prior in EnKF_PFL (whereas it was 12 h prior in EnKF_SND). The posterior error is almost the same as the prior error, but it is significantly larger than that of EnKF_SND since the same sounding observations (assimilated in EnKF_SND) are used to verify the results in all cases. There is apparently larger improvement in v (Fig. 10b). It is worth noting that though temperature is not observed, it is also improved relative to the reference EF below about 500 hPa through the flow-dependent background error covariance of the EnKF (light gray solid line in Fig. 10c).

Experiment 3DVAR_PFL (gray solid line in Fig. 10) shows a generally larger prior error than EnKF_PFL (light gray solid line in Fig. 10). It performs worse than EnKF_PFL at every layer for u, v, and q and at lower layers for T (Fig. 10). The prior RM-DTE of 3DVAR_PFL at 36 h is 1.75 m s^{-1} larger than that of EnKF_PFL (Fig. 6).

3) SURFACE DATA

In comparison with the sounding and profiler data assimilation results, even though there are many more surface stations in the inner domain, much less improvement is seen when only surface data is assimilated every 6 h in experiments EnKF_SFC and 3DVAR_SFC (Fig. 11). Only a small error reduction is seen in terms of the prior RM-DTE in EnKF_SFC relative to the reference EF (Fig. 6). As expected, error reduction in EnKF_SFC (versus EF) is mainly in the lower troposphere (light gray solid line in Fig. 11). Though less improvement is obtained in this case, EnKF_SFC still outperforms 3DVAR_SFC (gray solid line in Fig. 11). The prior RM-DTE of EnKF_SFC at 36 h is 1.94 m s^{-1} less than that of the 3DVAR_SFC. As in the profiler data assimilation, the posterior error is similar to the prior error in both EnKF_SFC and 3DVAR_SFC.

4) SOUNDING, PROFILER, AND SURFACE DATA

The results of experiments EnKF_ALL and 3DVAR_ALL, which assimilate all three types of observations at the aforementioned frequencies, show that utilization of all data types results in generally better performance than assimilating any individual source of observations (in terms of the prior error at 36 h; see Figs. 12 and 6). The RM-DTE in EnKF-All at 36 h is 4.25 m s^{-1}, which is 0.58 m s^{-1} less than that of the reference EF (Fig. 6). The most significant improvement comes from the middle troposphere (Fig. 12). The position of the MCV and its associated reflectivity are also noticeably improved (Fig. 2f). Again, the EnKF
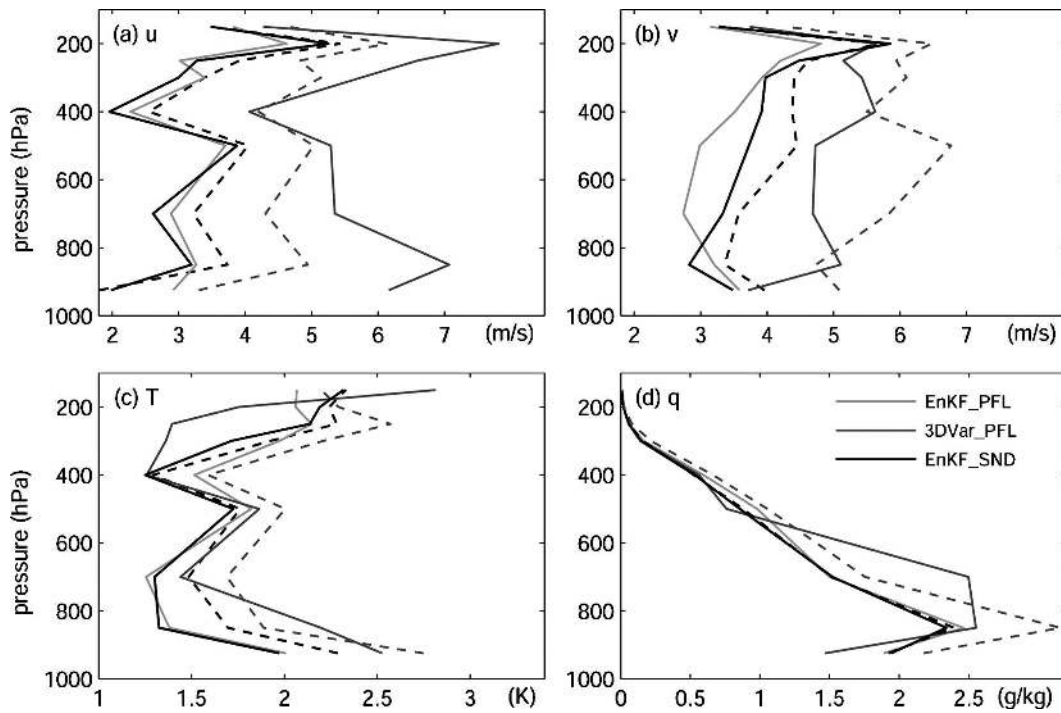
FIG. 10. Vertical distributions of the horizontally averaged RMSEs of (a) u, (b) v, (c) T, and (d) q at 36 h for the prior forecast of EnKF_PFL (light gray solid), 3DVAR_PFL (gray solid), EnKF_SND (black solid), and the RMSEs of the reference forecast DF (gray dashed) and EF (black dashed).
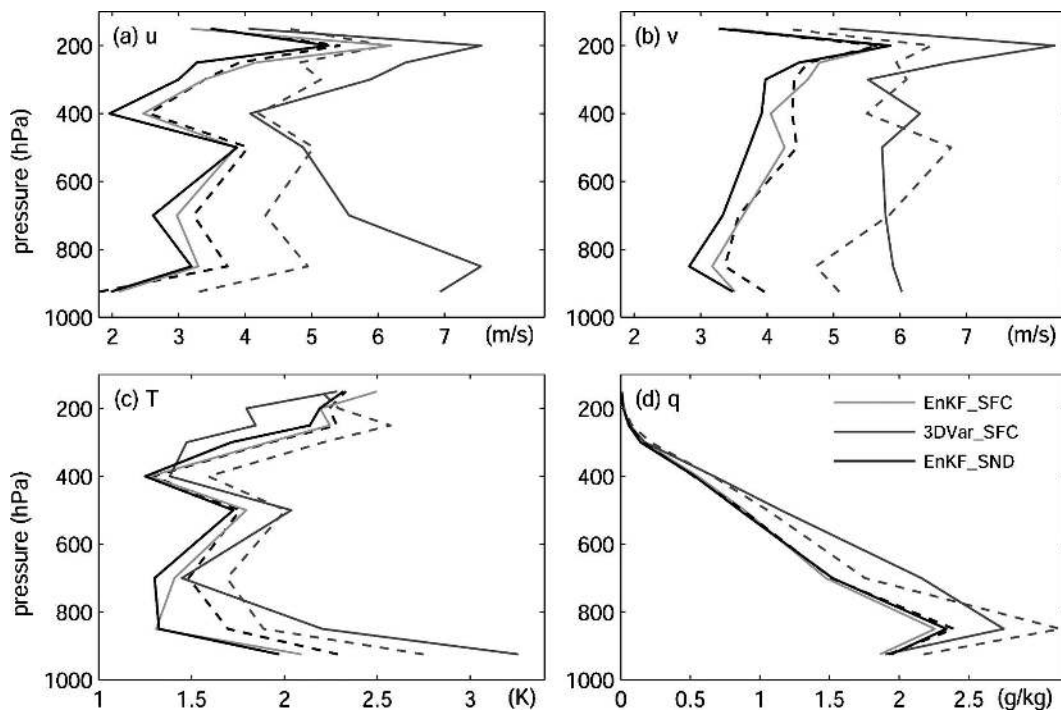

FIG. 11. As in Fig. 10 but for EnKF_SFC (light gray solid), 3DVAR_SFC (gray solid), and EnKF_SND (black solid).
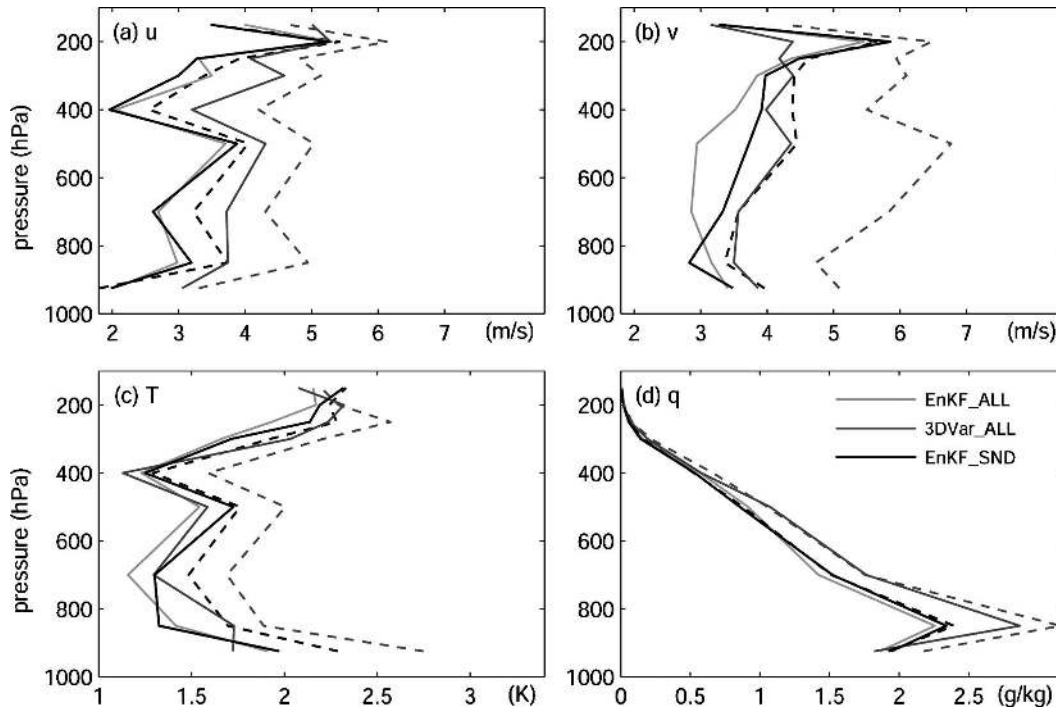
FIG. 12. As in Fig. 10 but for EnKF_ALL (light gray solid), 3DVAR_ALL (gray solid), and EnKF_SND (black solid).

outperforms 3DVAR for all u, v, T, and q (Fig. 12). The prior RM-DTE of 3DVAR_ALL at 36 h is 4.74 m s^{-1}, which is 0.49 m s^{-1} larger than that of EnKF_ALL, but the difference is smaller than that between EnKF_SND and 3DVAR_SND when less data are assimilated (Fig. 6).

5. Model error treatments in the EnKF

In real data assimilations, the model error can have an important impact on the performance of the assimilation technique. In this section, we examined the benefits of using a multischeme ensemble and covariance inflation for the treatment of forecast model errors. For simplicity, soundings are only assimilated every 12 h using EnKF_SND as a benchmark for comparison.

a. Multischeme ensemble

The impact of using a multischeme ensemble is investigated here to test the OSSE result in Part II that the EnKF performance can be improved through the use of different physical parameterization schemes in different ensemble members to account for model physics uncertainty. Experiment EnKF_multi uses a combination of three cumulus schemes [Kain–Fritsch (Kain and Fritsch 1993), Betts–Miller (Betts and Miller 1986), and Grell–Devenyi (Grell and Devenyi 2002)],

three PBL schemes [the YSU scheme (Noh et al. 2003), Mellor–Yamada–Janjić Eta Model (ETA; Janjić 2002), and the Medium-Range Forecast model (MRF; Hong and Pan 1996)], and three cloud physics schemes [Lin et al. (Lin et al. 1983), Thompson et al. (Thompson et al. 2004), and WSM six-class graupel (Hong et al. 2004)], which are near evenly distributed among the same number of ensemble members (Table 2). To differentiate the benefits of using the multischeme ensemble for better background error covariance from better prior estimates (or ensemble means), another reference forecast, EF_multi, is performed with the same multischeme configuration as that in EnKF_multi but without assimilating any observations.

The result shows that both the prior and posterior errors at 36 h of v, T, and q in EnKF_multi are decreased more than those in EnKF_SND (Fig. 4). The error reduction of 0.16 m s^{-1} comes from both the prior estimate using the multischeme ensemble forecast (light gray dashed line in Fig. 4) and the EnKF with better background error covariance (light gray solid in Fig. 4). The largest improvement is observed in T, which should be more closely related to the uncertainty in the physical parameterization schemes. EnKF_multi apparently has larger ensemble spread for all variables shown (light gray dotted line in Fig. 5) relative to that of EnKF_SND (black dotted line in Fig. 5).

TABLE 2. Model configuration of the experiment with multischeme ensemble EnKF_multi.

No. of members using a cumulus scheme and the scheme used	No. of members using a microphysics scheme and the scheme used	No. of members using the PBL scheme and the scheme used
13 Kain–Fritsch	4, Lin et al.	1, YSU; 2, ETA; 1, MRF
	4, Thompson et al.	1, YSU; 2, ETA; 1, MRF
	5, WSM six-class graupel	2, YSU; 2, ETA; 1, MRF
13 Betts–Miller	4, Lin et al.	1, YSU; 2, ETA; 1, MRF
	4, Thompson et al.	1, YSU; 2, ETA; 1, MRF
	5, WSM six-class graupel	2, YSU; 2, ETA; 1, MRF
14 Grell–Devenyi	4, Lin et al.	1, YSU; 2, ETA; 1, MRF
	5, Thompson et al.	2, YSU; 2, ETA; 1, MRF
	5, WSM six-class graupel	2, YSU; 2, ETA; 1, MRF

Forecasts starting from 1200 UTC 11 June with output at 30-min interval are also verified against dropsondes during 1600–1900 UTC (light gray lines in Fig. 8). Result shows that using a multischeme ensemble also improves the simulated MCV structure with a much better fit to the independent dropsonde observations for thermodynamic variables in the MCV area than that using a single-scheme ensemble.

b. Covariance inflation

Because of sampling and model errors, the EnKF may underestimate the analysis uncertainty, which could lead to filter divergence if untreated. Two common ways to cope with this problem are the multiplicative covariance inflation method (Anderson 2001) and the additive covariance inflation method (Hamill and Whitaker 2005; Houtekamer et al. 2005). However, both inflation methods may lead to excessive ensemble spread in data-sparse regions (Zhang et al. 2004).

As in Zhang et al. (2004) and described in section 2c, this study uses the covariance relaxation method [Eq. (1)] to inflate the background error covariance but avoid excessive spread. Three experiments with α of 0.0, 0.5, and 0.7, referred to as EnKF_mix0, EnKF_mix0.5, and EnKF_SND, respectively, are performed to test the EnKF sensitivity to the relaxation coefficient. Result shows that the relaxation (mixing) between the prior and posterior perturbations can draw the subsequent prior estimate closer to the observations, and a larger relaxation coefficient is necessary for this real-data application than the value of 0.5 used in the OSSEs (Part I; Part II). Overall, EnKF_SND (black solid line in Fig. 13) results in slightly smaller prior RMSEs than EnKF_mix0.5 (not shown). They both outperform EnKF_mix0 with no relaxation (gray solid line in Fig. 13).

Figure 13 also shows a consistent improvement from EnKF_mix0 to EnKF_SND and then to EnKF_multi (solid lines) possibly because of the correspondingly increasing ensemble spread, as shown by the dotted lines. This result indicates that proper covariance inflation or relaxation may improve the performance of the EnKF.

6. Tuning 3DVAR with ensembles

Results demonstrated in sections 4 and 5 show that the EnKF may benefit from both the use of ensemble forecasts to estimate the flow-dependent background error covariance and the use of an ensemble mean to estimate the prior. This section examines the possible impacts of adding some flow dependence into the BES and using ensemble-based state estimation on the performance of 3DVAR. In detail, one is the standard 3DVAR system using a newly generated BES but a single forecast for the prior estimate; the other is an ensemble-based 3DVAR, in which a short-term ensemble forecast is utilized to derive the prior estimate while the BES is either fixed or estimated with the same short-term ensemble (and thus has some flow dependency).

a. Impact of flow dependence in background error covariance

As introduced in section 2b, the WRF-3DVAR default background error covariance (the cv3 option) is calculated using a month-long GFS global model forecast via the NMC method. This could potentially be problematic because of error statistics calculated from a different model and a different grid size. The sensitivity of 3DVAR to the **B** matrix has been examined in Dee (1995), Fisher (2003), Derber et al. (2003), Hamill et al. (2003), and Buehner (2005), in which the **B** matrix is treated as inhomogeneous and anisotropic. This section investigates the possible benefits 3DVAR could receive from an ensemble-based BES, as is the case for the EnKF.
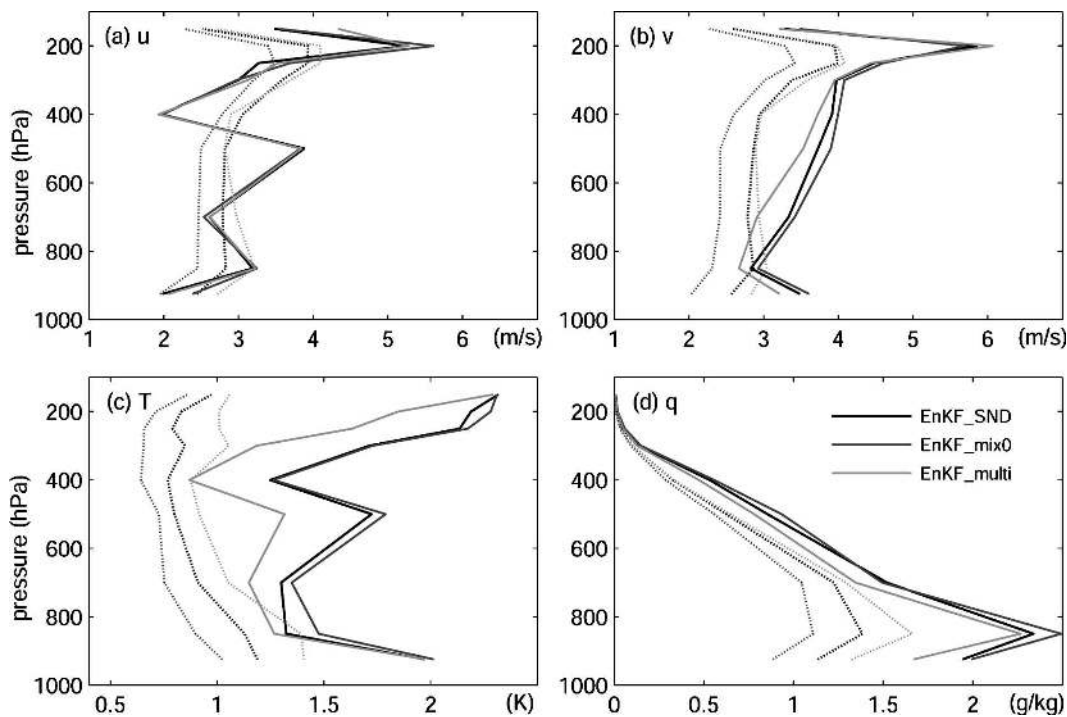
Using the cv5 option in WRF 3DVAR and the NMC

FIG. 13. As in Fig. 10 but for EnKF_mix0 (gray lines), EnKF_SND (black lines), and EnKF_multi (light gray lines).

method, experiment Var_nmcB generates the BES from 60 pairs of month-long (May 2003) 24- and 12-h forecast differences valid at the same time (every 12 h) with the WRF model configured in the same manner as with the reference DF. This method is expected to provide more reasonable BESs for scale, balance, and correlation structures than the one interpolated from the defaulted BES that was derived from a coarse-resolution global model (Lee and Barker 2005). However, in this case, the results of 3DVAR_SND and Var_nmcB are nearly indistinguishable in terms of the prior error at 36 h (Figs. 6 and 14).

Another way to generate the BES is to use a short-term ensemble forecast (Lorenc 2003; Lee and Barker 2005). Experiment Var_ensB utilizes a 40-member 12-h ensemble forecast valid at 0000 UTC 11 June to generate a BES that is fixed for subsequent assimilation cycles. In this case, the prior RM-DTE at 36 h is slightly smaller than that of 3DVAR_SND, which is consistent with other studies (e.g., Lee and Barker 2005). Vertical distributions of the prior RMSE show that the improvement comes mainly from u and v (solid light gray line in Fig. 14). The simulated reflectivity (Fig. 15a) is similar to that of 3DVAR_SND (Fig. 2d).

Experiment Var_evoB utilizes a 40-member 12-h ensemble to generate a different BES at every assimilation time (instead of being fixed as in Var_ensB). This

BES has some flow dependency but is still isotropic and mostly homogeneous. Its difference from the fixed BES lies in the time-variant correlation length scale and variance. Relative to 3DVAR_ensB, including some flow dependency in the BES results in only slight further improvement in terms of the prior error at 36 h (Figs. 6 and 14). Again, the surface structure of the MCV is similar to that in the previous standard 3DVAR experiments (Fig. 15b).

b. Impact of ensemble-based state estimate

As indicated in section 4, using an ensemble mean for state estimation may contribute a large part of the improvement of the EnKF over 3DVAR. In this section, two ensemble-based 3DVAR experiments, namely EnVar_ensB and EnVar_evoB (Table 3), are performed in this section to further examine the impacts of flow-dependent BES and of using an ensemble forecast mean to perform prior estimate. EnVar_ensB uses the mean of an ensemble initiated by 3DVAR to perform the state estimation. Each member goes through the forecast and analysis cycling independently with the same fixed BES as that in Var_ensB. The prior and posterior estimates at each assimilation time are simply the ensemble mean of the forecast and analysis ensembles. In EnVar_evoB, BES is generated from the
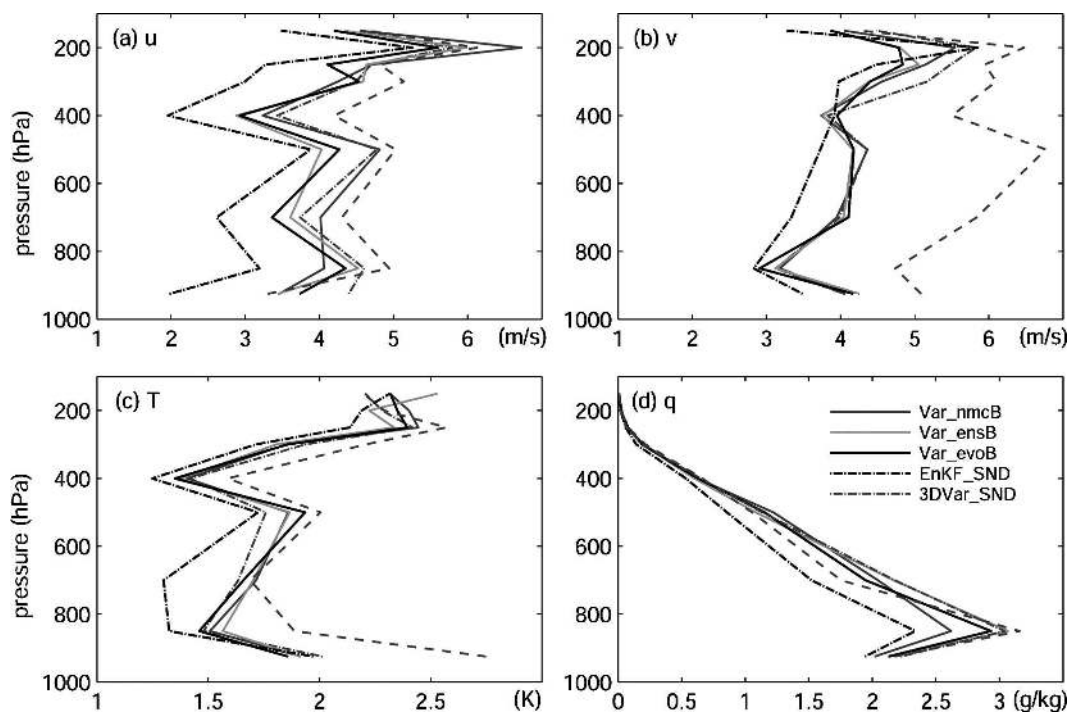
FIG. 14. Vertical distributions of the horizontally averaged prior RMSEs of (a) u, (b) v, (c) T, and (d) q at 36 h in Var_nmcB (gray solid), Var_ensB (light gray solid), and Var_evoB (black solid) in comparison with EnKF_SND (black dot–dashed). Also plotted are the RMSEs of the reference forecast DF (dashed) and the prior RMSEs of 3DVAR_SND (gray dot–dashed).

forecast ensemble at each assimilation time and it is thus time variant with some flow dependency involved.

The results show that the prior error of EnVar_ensB at 36 h (Figs. 6 and 16) is comparable to that of EnKF_SND, and it is significantly smaller than that of the standard 3DVAR experiments. The surface location of the MCV and its associated reflectivity pattern also apparently improve (Fig. 15c), becoming similar to those in EnKF_SND (Fig. 2e). This result suggests that the use of an ensemble mean can significantly improve the prior estimate and thus subsequent analyses. The improvement of EnVar_ensB over Var_ensB (0.5 m s^{-1}) is apparently larger than that of Var_evoB over Var_ensB (0.08 m s^{-1}), which indicates that using an ensemble mean to estimate the prior forecast and/or the posterior analysis is an important benefit of the EnKF.

In EnVar_evoB there is only slight further improvement in v (blue solid in Fig. 16) relative to EnVar_ensB. The overall prior RM-DTEs at 36 h in these two ensemble-based 3DVAR experiments are very similar. The intensity of the simulated reflectivity associated with the MCV is slightly improved (Fig. 15d). Similar to the comparison of Var_ensB and Var_evoB, the utilization of a time-variant BES in EnVar_evoB does not result in significant improvement over EnVar_ensB. Fi-

nally, the prior RM-DTE at 36 h of EnVar_evoB (4.47 m s^{-1}) is smaller than that of Var_evoB (4.9 m s^{-1}) (Fig. 6). This further confirms the benefits of using an ensemble to perform state estimation in ensemble-based data assimilation methods.

7. Summary and discussions

Through assimilating conventional observations including sounding, wind profiler, and surface data, the performance of a WRF-based EnKF is examined in comparison to WRF-3DVAR for the MCV event of 10–12 June 2003. Results show that the EnKF generally outperforms 3DVAR for this particular MCV case (in terms of the forecast RMSE initialized with the posterior analysis from the previous assimilation cycle). Part of the performance difference between these two methods is due to the use of an ensemble mean (which has a smoothing effect) in the EnKF instead of using a single unperturbed run in the 3DVAR for the RMSE verification.

The impact of different data types on the performance of both data assimilation methods is different. The prior RM-DTEs at 36 h are, respectively, 4.38, 4.25, and 4.71 m s^{-1} for the sounding, profiler, and surface
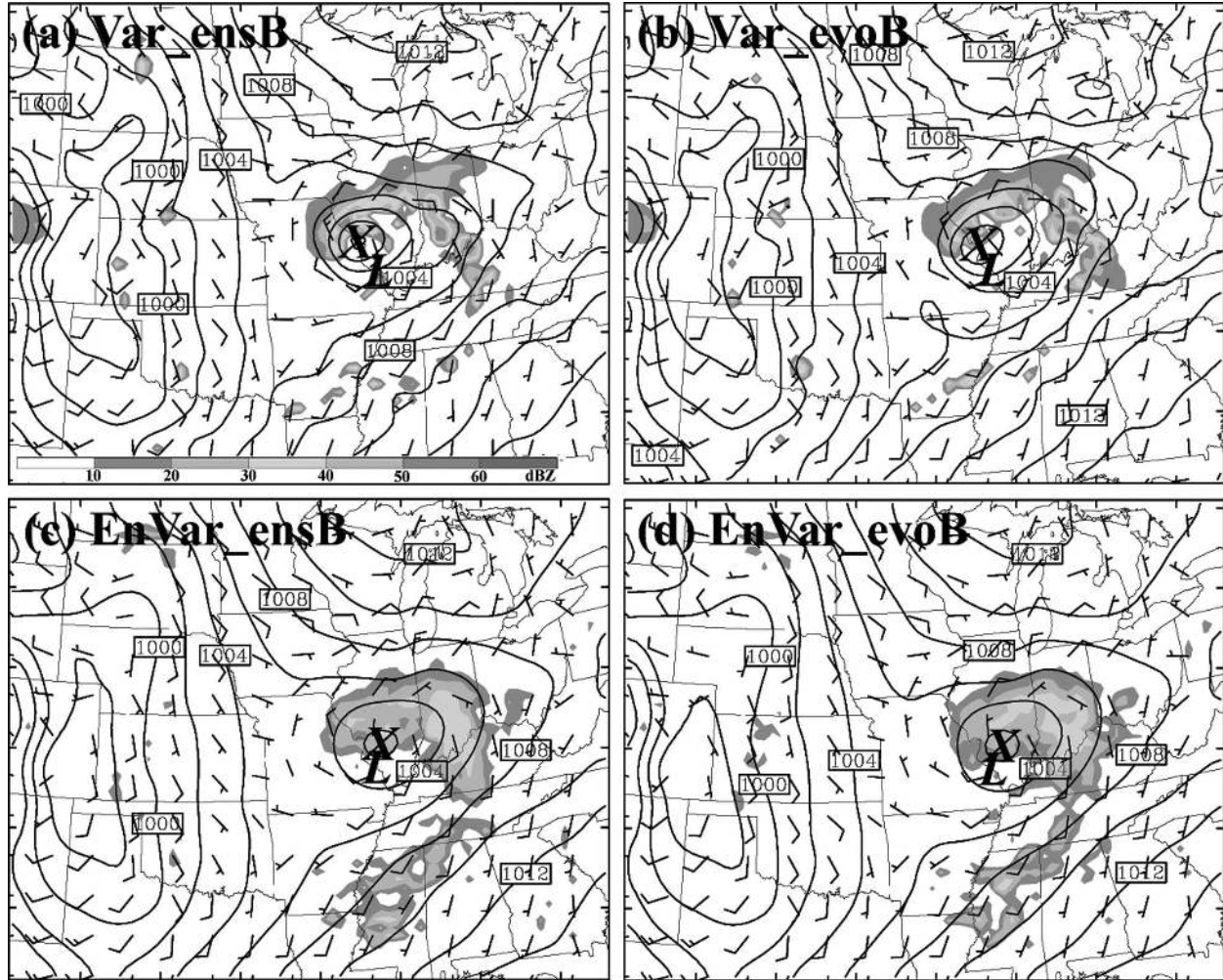
FIG. 15. As in Fig. 2 but for (a) Var_ensB, (b) Var_evoB, (c) EnVar_ensB, and (d) EnVar_evoB.

data assimilation experiments. These are smaller than the RM-DTEs for the reference forecasts (which are 5.96 m s^{-1} for the reference deterministic forecast and 4.83 m s^{-1} for the reference ensemble forecast). Similar to the OSSEs (Part I; Part II), larger improvements are seen in u, v, and T than in q. In each experiment with a single observation source, the EnKF shows consistently

better results than does 3DVAR. The prior RM-DTE at 36 h of the EnKF is about 0.5–1.5 m s^{-1} smaller than that of 3DVAR. The error growth rate of the forecast initiated from the 3DVAR analysis appears to be significantly larger than that from the EnKF analysis, possibly because of inappropriate error corrections by the 3DVAR at smaller scales where errors usually grow

TABLE 3. Experiment designs concerning the sensitivity of 3DVAR to different BESs.

| Groups	Expt	BES employed (the cv5 option)	Prior and posterior estimate
Standard 3DVAR	Var_nmcB	Fixed BES via the NMCmethod	Standard 3DVAR
	Var_ensB	Fixed BES via the first 12-h ensemble forecast (i.e., first 12 h of EF)	Standard 3DVAR
	Var_evoB	Evolving BES via preceding 12-h ensemble forecast	Standard 3DVAR
Ensemble-based 3DVAR	EnVar_ensB	Fixed BES as in Var_ensB; standard 3DVAR analysis for each member	Ensemble mean of the forecast and analysis ensemble
	EnVar_evoB	Evolving BES via preceding 12-h ensemble forecast; standard 3DVAR analysis for each member	Ensemble mean of the forecast and analysis ensemble
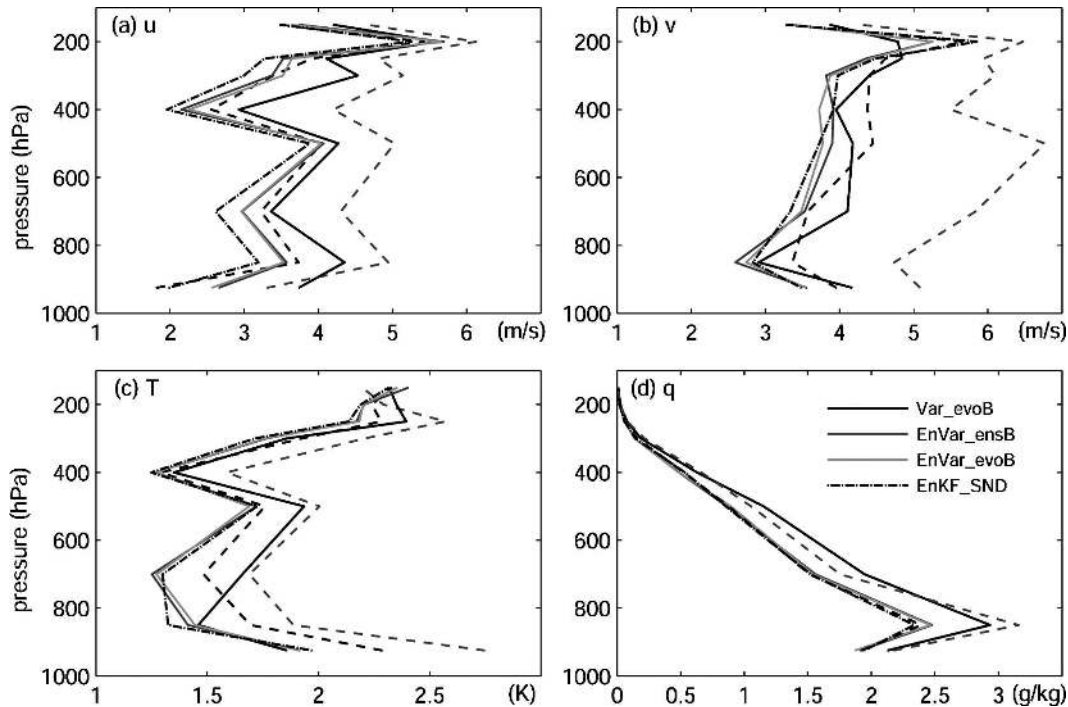
FIG. 16. Vertical distributions of the horizontally averaged prior RMSEs of (a) u, (b) v, (c) T, and (d) q at 36 h in Var_evoB (black solid), EnVar_ensB (gray solid), and EnVar_evoB (light gray solid) in comparison with EnKF_SND (black dot–dashed). Also plotted are the RMSEs of the reference forecast DF (gray dashed) and EF (black dashed).

faster. Both the EnKF and 3DVAR generally perform better when sounding, profiler, and surface observations are assimilated together than when each is assimilated separately. The EnKF again performs better than 3DVAR, though the difference becomes smaller than assimilating only sounding observations, suggesting that further reduction of the difference between the two methods may be expected when more observations, such as those from remote-sensing satellites, are assimilated.

Series experiments are implemented to examine the sensitivity of both the EnKF and 3DVAR to different background error covariances via sounding data assimilation. Examination of the impact of weighting coefficients in the covariance relaxation procedure of the EnKF shows that a value between 0.5 and 0.7 apparently gives better results than the case without relaxation. Similar to the OSSE experiments (Part II), using different combinations of physical parameterization schemes in different ensemble members can significantly improve the EnKF performance, especially for the thermodynamic variables.

The sensitivity of 3DVAR to various background error covariance methods is examined. Methods examined include the default cv3 BES option; option cv5, which is generated with month-long 24- and 12-h WRF

forecast differences for May 2003; and option cv5, which is generated with a 40-member 12-h forecast ensemble. Result shows that there are no significant performance differences among the different standard 3DVAR experiments. Slight improvement is observed when the background error statistics are generated at each data assimilation time with a 12-h forecast ensemble relative to the experiments with fixed background error statistics.

To examine the role of state estimation with an ensemble mean, two ensemble-based 3DVAR experiments with fixed and time-variant background error statistics are conducted. The two experiments perform similarly to each other but are apparently better than the standard 3DVAR experiments. Their performance levels are comparable to that of the EnKF, likely because of a better prior estimate via the use of an ensemble mean. Results also demonstrate that the utilization of an ensemble rather than a deterministic forecast results in a larger improvement than that obtained when one chooses a time-variant background error covariance over a fixed one. This suggests that the EnKF outperforms 3DVAR through not only its flow-dependent background error covariance but also its ensemble-based state estimation.

Last, note that all of the conclusions of the current

study are based on this particular MCV event, and they thus have their limitations. Longer-term experiments for this warm season and a winter season are under way and will be presented in a subsequent study.

REFERENCES

Aksoy, A., F. Zhang, J. W. Nielsen-Gammon, and C. C. Epifanio, 2005: Ensemble-based data assimilation for thermally forced circulations. *J. Geophys. Res.,* **110,** D16105, doi:10.1029/2004JD005718.

——, ——, and ——, 2006a: Ensemble-based simultaneous state and parameter estimation in a two-dimensional sea-breeze model. *Mon. Wea. Rev.,* **134,** 2951–2970.

——, ——, and ——, 2006b: Ensemble-based simultaneous state and parameter estimation with MM5. *Geophys. Res. Lett.,* **33,** L12801, doi:10.1029/2006GL026186.

Anderson, J. L., 2001: An ensemble adjustment Kalman filter for data assimilation. *Mon. Wea. Rev.,* **129,** 2884–2903.

Barker, D. M., 2005: Southern high-latitude ensemble data assimilation in the Antarctic Mesoscale Prediction System. *Mon. Wea. Rev.,* **133,** 3431–3449.

——, W. Huang, Y.-R. Guo, A. J. Bourgeois, and Q. N. Xiao, 2004: A three-dimensional variational data assimilation system for MM5: Implementation and initial results. *Mon. Wea. Rev.,* **132,** 897–914.

Benjamin, S., B. E. Schwartz, E. J. Szoke, and S. E. Koch, 2004: The value of wind profiler data in U.S. weather forecasting: Case studies. *Bull. Amer. Meteor. Soc.,* **85,** 1871–1886.

Betts, A. K., and M. J. Miller, 1986: A new convective adjustment scheme. Part II: Single column tests using GATE wave, BOMEX, and arctic air-mass data sets. *Quart. J. Roy. Meteor. Soc.,* **112,** 693–709.

Buehner, M., 2005: Ensemble-derived stationary and flow-dependent background-error covariances: Evaluation in a quasi-operational NWP setting. *Quart. J. Roy. Meteor. Soc.,* **131,** 1013–1043.

Caya, A., J. Sun, and C. Snyder, 2005: A comparison between the 4DVAR and the ensemble Kalman filter techniques for radar data assimilation. *Mon. Wea. Rev.,* **133,** 3081–3094.

Chessa, P. A., G. Ficca, M. Marrocu, and R. Buizza, 2004: Application of a limited-area short-range ensemble forecast system to a case of heavy rainfall in the Mediterranean region. *Wea. Forecasting,* **19,** 566–581.

Daley, R., and R. Menard, 1993: Spectral characteristics of Kalman filter systems for atmospheric data assimilation. *Mon. Wea. Rev.,* **121,** 1554–1565.

Davis, C. A., and S. B. Trier, 2007: Mesoscale convective vortices observed during BAMEX. Part I: Kinematic and thermodynamic structure. *Mon. Wea. Rev.,* **135,** 2029–2049.

——, and Coauthors, 2004: The Bow-Echo and MCV Experiment (BAMEX): Observations and opportunities. *Bull. Amer. Meteor. Soc.,* **85,** 1075–1093.

Dee, D. P., 1995: On the estimation of error covariance parameters for atmospheric data assimilation. *Mon. Wea. Rev.,* **123,** 1128–1145.

Derber, J. C., P. Van Delst, X. Su, X. Li, K. Okamoto, and R. Treadon, 2003: Enhanced use of radiance data in NCEP data assimilation system. *Proc. 13th Int. TOVS Study Conf.,* St. Adele, QC, Canada, Int. TOVS Working Group, 52–60. [Available online at http://cimss.ssec.wisc.edu/itwg/itsc/itsc13/proceedings/session1/1_8_derber.pdf.]

Dirren, S., R. D. Torn, and G. J. Hakim, 2007: A data assimilation case study using a limited-area ensemble Kalman filter. *Mon. Wea. Rev.,* **135,** 1455–1473.

Dowell, D. C., F. Zhang, L. J. Wicker, C. Snyder, and N. A. Crook, 2004: Wind and temperature retrievals in the 17 May 1981 Arcadia, Oklahoma, supercell: Ensemble Kalman filter experiments. *Mon. Wea. Rev.,* **132,** 1982–2005.

Evensen, G., 1994: Sequential data assimilation with a nonlinear quasi-geostrophic model using Monte Carlo methods to forecast error statistics. *J. Geophys. Res.,* **99,** 10 143–10 162.

——, 2003: The ensemble Kalman filter: Theoretical formulation and practical implementation. *Ocean Dyn.,* **53,** 343–367.

Fisher, M., 2003: Background error covariance modelling. *Proc. Seminar on Recent Developments in Data Assimilation for Atmosphere and Ocean,* Reading, United Kingdom, ECMWF, 45–64.

Fujita, T., D. J. Stensrud, and D. C. Dowell, 2005: Surface data assimilation using an ensemble Kalman filter approach with initial condition and model physics uncertainties. Preprints, *11th Conf. on Mesoscale Processes,* Albuquerque, NM, Amer. Meteor. Soc., 1M.3.

Gaspari, G., and S. E. Cohn, 1999: Construction of correlation functions in two and three dimensions. *Quart. J. Roy. Meteor. Soc.,* **125,** 723–757.

Grell, G. A., and D. Devenyi, 2002: A generalized approach to parameterizing convection combining ensemble and data assimilation techniques. *Geophys. Res. Lett.,* **29,** 1693, doi:10.1029/2002GL015311.

Hamill, T. M., 2006: Ensemble-based atmospheric data assimilation. *Predictability of Weather and Climate,* T. Palmer and R. Hagedorn, Eds., Cambridge Press, 124–156.

——, and C. Snyder, 2000: A hybrid ensemble Kalman filter–3D variational analysis scheme. *Mon. Wea. Rev.,* **128,** 2905–2919.

——, and J. S. Whitaker, 2005: Accounting for the error due to unresolved scales in ensmeble data assimilation: A comparison of different approaches. *Mon. Wea. Rev.,* **133,** 3132–3147.

——, C. Snyder, and J. S. Whitaker, 2003: Ensemble forecasts and the properties of flow-dependent analysis-error covariance singular vectors. *Mon. Wea. Rev.,* **131,** 1741–1758.

Hawblitzel, D. P., F. Zhang, Z. Meng, and C. A. Davis, 2007: Probabilistic evaluation of the dynamics and predictability of a mesoscale convective vortex event of 10–13 June 2003. *Mon. Wea. Rev.,* **135,** 1544–1563.

Hong, S.-Y., and H.-L. Pan, 1996: Nonlocal boundary layer vertical diffusion in a medium-range forecast model. *Mon. Wea. Rev.,* **124,** 2322–2339.

——, J. Dudhia, and S.-H. Chen, 2004: A revised approach to ice microphysical processes for the parameterization of clouds and precipitation. *Mon. Wea. Rev.,* **132,** 103–120.

Houtekamer, P. L., and H. L. Mitchell, 1998: Data assimilation using an ensemble Kalman filter technique. *Mon. Wea. Rev.,* **126,** 796–811.

——, and ——, 2001: A sequential ensemble Kalman filter for atmospheric data assimilation. *Mon. Wea. Rev.,* **129,** 123–137.

——, ——, G. Pellerin, M. Buehner, M. Charron, L. Speak, and B. Hansen, 2005: Atmospheric data assimilation with an ensemble Kalman filter: Results with real observations. *Mon. Wea. Rev.,* **133,** 604–620.

Janjić, Z. I., 2002: Nonsingular implementation of the Mellor–Yamada level 2.5 scheme in the NCEP Meso Model. NCEP Office Note, 437, 61 pp.

Kain, J. S., and J. M. Fritsch, 1993: Convective parameterization for mesoscale models: The Kain–Fritcsh scheme. *The Representation of Cumulus Convection in Numerical Models, Meteor. Monogr.,* No. 46, Amer. Meteor. Soc., 165–170.

Keppenne, C. L., and M. M. Rienecker, 2002: Initial testing of a massively parallel ensemble Kalman filter with the Poseidon isopycnal ocean general circulation model. *Mon. Wea. Rev.,* **130,** 2951–2965.

Lee, M. S., and D. M. Barker, 2005: Background error statistics in 3DVAR derived from WRF ensembles. *Abstracts, WRF/MM5 Users' Workshop,* Boulder, CO, NCAR, 3.20.

Lin, Y.-L., R. D. Farley, and H. D. Orville, 1983: Bulk parameterization of the snow field in a cloud model. *J. Climate Appl. Meteor.,* **22,** 1065–1092.

Lorenc, A. C., 2003: The potential of the ensemble Kalman filter for NWP—A comparison with 4Dvar. *Quart. J. Roy. Meteor. Soc.,* **129,** 3183–3203.

Meng, Z., and F. Zhang, 2007: Tests of an ensemble Kalman filter for mesoscale and regional-scale data assimilation. Part II: Imperfect model experiments. *Mon. Wea. Rev.,* **135,** 1403–1423.

Mitchell, H. L., P. L. Houtekamer, and G. Pellerin, 2002: Ensemble size, balance, and model-error representation in an ensemble Kalman filter. *Mon. Wea. Rev.,* **130,** 2791–2808.

Noh, Y., W.-G. Cheon, S.-Y. Hong, and S. Raasch, 2003: Improvement of the K-profile model for the planetary boundary layer based on large eddy simulation data. *Bound.-Layer Meteor.,* **107,** 401–427.

Parrish, D. F., and J. C. Derber, 1992: The National Meteorological Center's spectral statistical-interpolation analysis system. *Mon. Wea. Rev.,* **120,** 1747–1763.

Skamarock, W. C., J. B. Klemp, J. Dudhia, D. O. Gill, D. M. Barker, W. Wang, and J. G. Powers, 2005: A description of the Advanced Research WRF version 2. NCAR Tech. Note NCAR/TN-468+STR, 88 pp.

Snyder, C., and F. Zhang, 2003: Assimilation of simulated Doppler radar observations with an ensemble Kalman filter. *Mon. Wea. Rev.,* **131,** 1663–1677.

Thompson, G., R. M. Rasmussen, and K. Manning, 2004: Explicit forecasts of winter precipitation using an improved bulk microphysics scheme. Part I: Description and sensitivity analysis. *Mon. Wea. Rev.,* **132,** 519–542.

Tong, M., and M. Xue, 2005: Ensemble Kalman filter assimilation of Doppler radar data with a compressible nonhydrostatic model: OSS experiments. *Mon. Wea. Rev.,* **133,** 1789–1807.

Torn, R. D., G. J. Hakim, and C. Snyder, 2006: Boundary conditions for limited-area ensemble Kalman filters. *Mon. Wea. Rev.,* **134,** 2490–2502.

Trier, B. S., and A. C. Davis, 2007: Mesoscale convective vortices observed during BAMEX. Part II: Influences on secondary deep convection. *Mon. Wea. Rev.,* **135,** 2051–2075.

——, C. A. Davis, D. A. Ahijevych, M. L. Weisman, and G. H. Bryan, 2006: Mechanisms supporting long-lived episodes of propagating nocturnal convection within a 7-day WRF model simulation. *J. Atmos. Sci.,* **63,** 2437–2461.

Whitaker, J. S., and T. M. Hamill, 2002: Ensemble data assimilation without perturbed observations. *Mon. Wea. Rev.,* **130,** 1913–1924.

——, G. P. Compo, X. Wei, and T. M. Hamill, 2004: Reanalysis without radiosondes using ensemble data assimilation. *Mon. Wea. Rev.,* **132,** 1190–1200.

——, T. M. Hamill, X. Wei, Y. Song, and Z. Toth, 2008: Ensemble data assimilation with the NCEP Global Forecast System. *Mon. Wea. Rev.,* **136,** 463–482.

Xiao, Q., and J. Sun, 2007: Multiple-radar data assimilation and short-range quantitative precipitation forecasting of a squall line observed during IHOP_2002. *Mon. Wea. Rev.,* 3381–3404.

Zhang, F., 2005: Dynamics and structure of mesoscale error covariance of a winter cyclone estimated through short-range ensemble forecasts. *Mon. Wea. Rev.,* **133,** 2876–2893.

——, and C. Snyder, 2007: Ensemble-based data assimilation. *Bull. Amer. Meteor. Soc.,* **88,** 565–568.

——, ——, and J. Sun, 2004: Impacts of initial estimate and observation availability on convective-scale data assimilation with an ensemble Kalman filter. *Mon. Wea. Rev.,* **132,** 1238–1253.

——, Z. Meng, and A. Aksoy, 2006: Tests of an ensemble Kalman filter for mesoscale and regional-scale data assimilation. Part I: Perfect model experiments. *Mon. Wea. Rev.,* **134,** 722–736.

Zhang, S., and J. L. Anderson, 2003: Impact of spatially and temporally varying estimates of error covariance on assimilation in a simple atmospheric model. *Tellus,* **55A,** 126–147.